This is a repository copy of *Evaluation of the potential of retrofitting a coal power plant to oxy-firing using CFD and process co-simulation*.

White Rose Research Online URL for this paper:
http://eprints.whiterose.ac.uk/84029/

Version: Accepted Version

Evaluation of the potential of retrofitting a coal power plant to oxy-firing using CFD and process co-simulation

Fei Y.[a], Black S., Szuhánszki J.[a], Ma L.[a,*], Ingham D.B.[a], Stanger P.[b], Pourkashanian M.[a]

a *Energy Technology and Innovation Initiative, Faculty of Engineering, University of Leeds, Leeds LS2 9JT, UK*
b *Process Systems Enterprise Ltd, 26-28 Hammersmith Grove, London W6 7HA, UK*

Abstract:

In this paper, a new approach has been developed for estimating the potential of retrofitting an existing power plant to oxy-firing and determining the safe operation regime of the boiler under enriched oxy-combustion. A Computational Fluid Dynamics (CFD) technique has been employed to simulate the complex coal combustion and heat transfer to the furnace water walls and heat exchangers under air-firing and oxy-firing conditions. A set of reduced order models (ROMs) have been developed to link the CFD predictions to the efficient whole plant process models in order to simulate the performance of the power plant under different load and oxygen enrichment conditions if retrofitted to oxy-firing. The simulations of a 500MW$_e$ power plant unit indicate that it is possible to retrofit it to oxy-firing without affecting the overall performance of the unit. Similar heat transfer characteristics and steam generation can be achieved to those under air-firing, although the temperature of the boiler wall may increase after retrofitting. The upper limits for the oxygen enrichment at different power loads are identified and the feasible oxygen concentration range within 25%-27% is suggested for the oxy-coal operation of this retrofitted power plant investigated. However, the peak temperature on the superheater platen 2 may increase in the oxy-coal mode at high power load beyond 450MW$_e$. If the tube material cannot endure the temperature increase, then an upgrade on the material is required.

Keywords: CFD, Combustion, Coal, Oxy-coal, Process simulation, Reduced order model (ROM)

1. Introduction

Coal is expected to continually play an important role in the world energy mix in the foreseeable future. However, burning coal contributes significantly to the global CO_2 emission and thus a major issue that has to be addressed in the power generation sector. Oxy-coal combustion is one of the most promising technology options that can be applied to both new-build and retrofitting of an existing power plant for carbon capture and storage (CCS). Predicting the performance of a retrofitted plant can play an important role in reducing the technical risk of future integration of CCS with existing power plants.

Unlike the conventional air-firing process, oxy-combustion takes place in a mixture of O_2 and CO_2 or recycled flue gas. This produces a high concentration CO_2 (>85%) in the flue gas stream that is almost ready for compression and sequestration after purification. Because of the changes in the gas compositions in the furnace, the temperature and heat transfer characteristics of the boiler are expected to be very different from air-firing. From the view point of the economic and safe operation of the plant, it is desirable that these changes do not deviate too much from designed air-firing conditions after retrofitting of an existing conventional power plant [1]. Whole plant process computer simulation as a flexible and economic tool has been widely employed in modelling power plant operation for both air and oxy-fired scenarios [2-4]. However, a major challenge for large scale whole plant process simulation lies in the difficulty in accurately modelling the combustion and thermal characteristics of the boiler where complex fluid dynamics dominates and the heat transfer characteristics are strongly affected by the fundamental properties of the oxidant gas and boiler geometries. Computational Fluid Dynamics (CFD) is effective in modelling the details of the combustion process and can produce accurate representations of the temperature and heat transfer distributions in the combustion boiler and this has been extensively documented in the literature [5-14]. However, CFD is incapable of modelling all components of a complex power plant efficiently and economically, in particular in an integrated manner. In order to take advantages of the efficiency of process modelling and accuracy of the CFD modelling techniques, we have linked the CFD simulations to a power plant model of a 500MW$_e$ pulverised coal combustion boiler in one of our previous papers [18], in addition to the attempts made by [15-17] for air-firing systems. In this paper, in order to investigate the potential of retrofitting an existing power plant to oxy-firing and to predict the safe operational regime that matches the designed air-firing conditions, an efficient reduced order

model (ROM) has been developed to combine the CFD simulations with the whole plant process simulations.

The Didcot-A coal fired power plant [19] has been taken in this paper to be retrofitted to oxy-firing, see Fig. 1. The boiler has been modelled by the CFD approach while other components, such as convective heat exchangers, steam turbines, ASU and CPU, are modelled by the process simulation models. Reduced order models (ROMs) for the heat transfer in the boiler have been developed based on a series of properly designed CFD simulations that accurately represent the thermal characteristics of the furnace in the integrated whole plant simulation.. Finally, with the newly developed integrated full plant model, the range of oxygen concentrations at the boiler inlet for oxy-coal operating of the power plant are identified in order to match the heat transfer, the steam generation and the steam temperatures inside the superheaters to those of the designed air-coal firing conditions.

2. The case studied

Didcot-A was designed to generate 2,000MW$_e$ of electricity. It consists of four 500MW$_e$ coal-fired generating units. In this paper one of the 500MW$_e$ units is "retrofitted" to oxy-coal firing by adding a cryogenic ASU, a CPU and a flue gas recycle loop. The layout of the original power generating unit, and the added ASU and CPU for oxy-fuel retrofit is shown in the dash-lined boxes on the top and bottom, respectively, in Fig. 1. The functionalities of the essential components are summarized in Table 1 and a set of proportional-integral (PI)/proportional-integral-derivative (PID) controllers has been employed to control the behaviour of the system in order to achieve the required working scenarios of the power plant and these PI/PID controllers are described in Table 2.
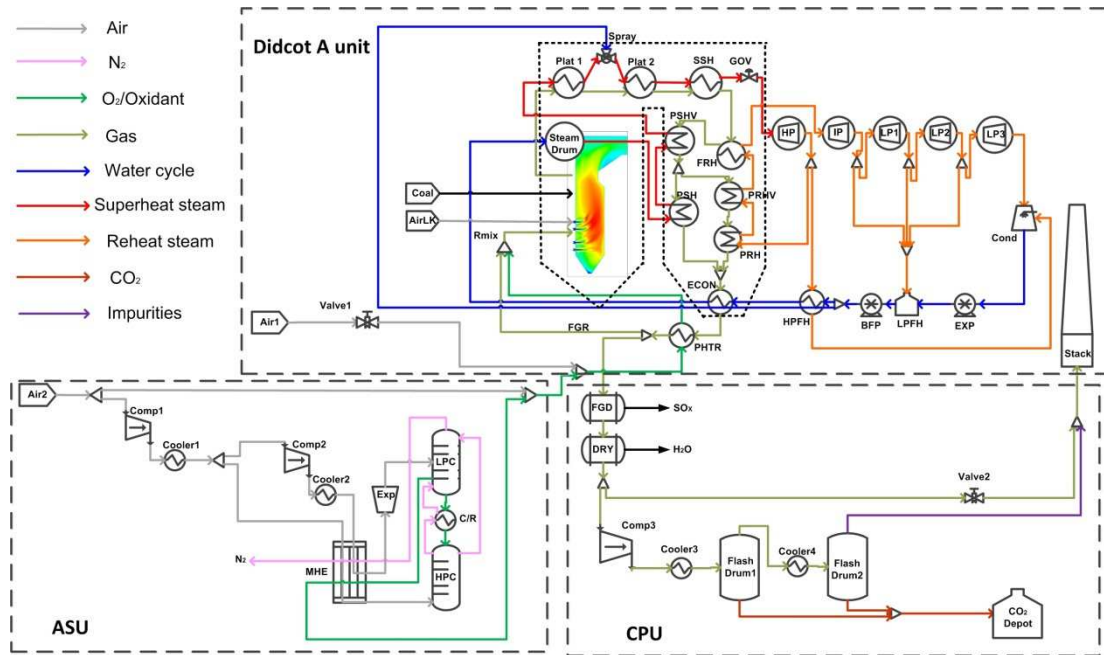
Fig. 1 Layout of the original power generating unit, ASU and CPU for oxy-fuel retrofit.

The detailed processes of the gas side and the water/steam side of the Didcot-A power plant have been described in our previous publication [21], therefore only a brief introduction in relation to Fig. 1 is given in this section. The material streams are defined as "Air", "N_2", "O_2/Oxidant", "Gas", "Water cycle", "superheat steam", "reheat steam", "CO_2" and "impurities" according to the main materials contained in the stream. The main reason for defining specific material types is in order to show clearly the different pipe lines and their usages. Several mixers and splitters are also used in the process.

In oxy-firing, an ASU is employed to generate oxygen, which is a typical double column design [22] and the oxygen purity can be adjusted between 95% and 98.5%. Typical oxy-coal combustion requires the purity of the oxygen stream to be no less than 95% by volume [23]. The oxygen purity has been set as 95% and maintained the same in the boiler CFD simulations. This oxygen stream is then mixed with a fraction of the recycled flue gas at a desired oxygen concentration before being transported to the furnace for the coal combustion. Here there is intensive heat transfer between the hot combustion products and water walls and the platen heat exchangers through radiation and convection. The hot flue gas then travels through the radiative superheaters, exchanging heat to the steam cycle. Due to the arrangement of the tube superheaters, a fraction of the flue gas may bypass the platen superheaters. After the first convective heat exchanger (PSHV), the primary vertical superheater, the gas flow is split in the backpass between the superheat exchangers (Platen 1, Platen 2 and SSH) and the reheat exchangers (FRH), and then mixed before the economiser (ECON).

The feedwater flow supplied by the economiser to the drum is required in order to match the steam generation. Water is circulated around the waterwalls, where it is heated and partially evaporated. The waterwall loop is a natural circulation system driven by the deferential density of the water. As a sub-critical system, the steam drum operates at a pressure of 178 bars for the full load (500MWe) and 165 bars for part load (350MWe), and the steam generated from the drum is saturated. The required steam generation and the plant power output depends on the thermal input that is regulated by a PI controller.

The post processing of the flue gas involves an FGD unit, which removes SO_x, and a dryer, which removes moisture. Further, the purity of the CO_2 stream for storage is required above 95% [23] and therefore a CPU is required to purify the CO_2 stream.

Table 1 Essential components and simple instructions for the full plant model.

Names of the components	Simple instructions
Air1, Air2, AirLK	Air1: air source for the furnace; Air2: air source for the air separation unit; AirLK: air source for the air leakage.
Comp	Compressor
Cooler	Used to cool down the inlet stream
Cond	Steam condenser
CO_2 Depot	A temporary deposit tank for the captured CO_2
C/R	Condenser and Reboiler
DRY	Flue gas drying
EXP, BFP	Pumps, pressurize the feeding water
Exp	Expander, expand the high pressure air
ECON	Economiser, preheat the feed water
Furnace	Furnace
FGD	Flue gas desulphurisation
FGR	Flue gas recycle loop
Flash Drum	Used to separate the impurities from the CO_2 stream

GOV	Governor valve, control the steam mass flow rate into the high pressure steam turbine
HPC, LPC	HPC: high pressure column LPC: low pressure column
PHTR	Preheater, heating the inlet air or oxygen
Plat1, Plat2, SSH, FRH	Radiative superheaters Platen1, Platen2, SSH, FRH
PSHV, PSH, PRHV, PRH	Convective heat exchangers
HP, IP, LP1, LP2, LP3	Steam turbines, HP: high pressure, IP: intermediate pressure, LP: low pressure
MHE	Main heat exchanger for the air separation unit
Rmix	Recycle mix, mix the recycled flue gas with oxygen
Spray	Water spray, control the temperature of the steam goes into the Plat2
Steam Drum	Steam Drum, generating the high pressure steam
Stack	Exhaust the flue gas from air-coal firing or the impurities in the CO_2 stream
Valve1, Valve2	Valve1: opens only when the boiler functions under the air-coal condition; Valve2: opens only when the CO_2 stream is not pure enough for compression and purification

Table 2 PI/PID controllers used in the full plant model.

PI/PID controllers used	Usage of the PI/PID controllers
Coal feed rate PI controller	The coal feed rate is adjusted so as to achieve the required pressure in the steam drum for the target power output.
Feed water rate PI controller	The mass flow rate of the feed water into the steam drum is controlled so as to maintain the required water level in the steam drum.
Governor valve PI controller	The open fraction of the valve is controlled so that the mass flow rate of the steam into the steam turbines, and thus the required power output, can be achieved.
Air1, Air2 mass flow rate PI controller	The oxygen concentration at the exit is measured. When the power plant functions under air-coal firing status, the mass flow rate from the Air1 that goes into the furnace is controlled. When the power plant functions under oxy-coal conditions, the source of Air1 is closed and the mass flow rate from the Air2 that goes into the ASU is controlled.
ASU bypass PID controller	The oxygen concentration in the oxygen product is measured, and from this measurement the fraction of inlet oxidant bypassing the ASU is adjusted.
HPC reboiler level PID controller	The liquid level in the reboiler of the high pressure column is measured. From this the mass flow rate of the liquid going out of the reboiler is controlled.

FGR PID controller	The oxygen concentration of the oxidant going into the furnace is measured. From this, the amount of the recycled flue gas is controlled and mixed with the inlet oxygen.
Water sprayer PID controller	The water sprayed into the steam between the Plat1 and the Plat2 is adjusted in order to control the temperature of the steam that goes into the Plat2.

3. Co-simulation of the whole plant

As discussed in Section 1, in order to take the advantages of the efficiency of the process modelling and the accuracy of the detailed CFD modelling, a co-simulation strategy has been employed. In the traditional process modelling of a power plant, the heat transfer to the water wall and superheat components are usually calculated using empirical equations. For oxy-fuel combustion, there are no such empirical equations that may be employed with confidence but a ROM based on CFD modelling is becoming a viable method to address this problem. Thus it was decided that the commercial process simulation software gPROMS 3.6.0 combined with a CFD based ROM should be employed for the whole power plant simulation. The heat transfer to the steam side inside the steam generation/superheat components of the boiler, up to the exit of the FRH, is simulated using a 3D CFD approach to generate necessary ROMs to be incorporated in the plant simulation, and the rest of the steam cycle and other process units, such as convective heat exchangers, columns, pumps, and compressors are modelled using process models based on first principle models.

The CFD based ROMs for oxy-coal combustion take the oxygen concentration and coal feed rate as dependent variables and these ROMs are created from CFD simulations using the Kriging method [20], which cover different thermal inputs and oxygen concentrations. These fast ROMs account for the heat transfer to different radiant parts of the boiler, the gas temperature leaving the boiler and the maximum temperature on the metal wall of the boiler. In the full plant process model, the ROMs are used to drive the steam generation and superheating in the main radiative superheaters, the gas temperature leaving the boiler drives the downstream convective heat exchange process and the maximum temperature on the waterwall provides reference for evaluating the boiler safety.

3.1 Essential component models for the whole plant simulation

The heat transfer characteristics and steam generation are critical to the power plant. Models for the natural circulation, superheat exchangers and convective heat exchangers are described in this section.

3.1.1 The natural circulation model

The natural circulation model is based on the work reported by Bhambare[24], Hasan[25], Adam[26] and Åström[27]. The heat transfer absorbed by the water wall drives the natural circulation of the steam/water. The heat released from the coal combustion is transferred to the water walls, e.g. the downcomer and the riser surrounding the boiler. The mass flow rate $\dot{m}_{XR}$ of the water, leaving the riser and going into the drum, is modelled as a function of the pressure drop in the riser as follows:

$$\dot{m}_{XR} = K_{XR}\sqrt{(P_1 - P - g\rho_{XR}z)\rho_{XR}} \tag{1}$$

where K_{XR} is an empirical constant that relates the pressure drop in the riser to the water flow rate. P_1 and P are the pressure at the bottom and top of the riser, resepectively, g is the gravity, ρ_{XR} is the density of the water and z is the height.

The dynamic mass balance for the flow in the risers is described by:

$$\dot{m}_{WDC} - \dot{m}_{XR} = V_R \frac{d\rho_{XR}}{dt} \tag{2}$$

where $\dot{m}_{WDC}$ is the mass flow rate at the exit of the downcomer and V_R is the volume of the riser tubes.

The dynamic mass balance for the steam in the steam drum is given by:

$$\dot{m}_{XR}X_R - \dot{m}_S = (V_T - V_W)\frac{d\rho_S}{dt} \tag{3}$$

where $\dot{m}_S$ is the mass flow rate of the steam leaving the steam drum, V_T is the total volume of the steam drum, V_W is the volume occupied by the water in the steam drum and X_R is the mass fraction of steam in the mixture at the riser exit.

The dynamic mass balance for the water in the steam drum is given by:

$$\frac{dM_W}{dt} = \dot{m}_f + \dot{m}_{XR}(1 - X_R) - \dot{m}_{WDC} \tag{4}$$

where M_W is the total mass of the water in the steam drum and $\dot{m}_f$ is the mass flow rate of the feeding water into the steam drum.

The dynamic enthalpy balance for the fluid in the riser is given by:

$$\dot{m}_{XR}(h_{WDC} - h_{XR}) + \dot{Q}_{XR}(\dot{m}_{coal}, y_{ox}) = V_R \frac{dh_{XR}}{dt} \qquad (5)$$

where h_{WDC} and h_{XR} are the mass specific enthalpies of the mixture at the exit of the downcomer and the exit of the riser, respectively. $\dot{Q}_{XR}$ is the heat transfer rate to the water/steam inside the water wall which will be calculated, based on the CFD modelling through the reduced order model (ROM) developed in Section 4.3, as a function of the coal feed rate $\dot{m}_{coal}$ and the volume concentration of oxygen y_{ox} entering the boiler.

3.1.2 The superheater/reheater model

A single model will be employed for the heat transfer to the steam side of the superheaters platen 1, platen 2, SSH and the reheater FRH. It should be noted that a fraction of the combustion gas in fact bypasses platen 1 and platen 2 and this can be easily understood by investigating the layout of the hanging superheaters shown in Fig. 1 and since the bypass fractions are difficult to obtain, the gas side is not modelled. This is considered not to affect the heat transfer predictions.

The dynamic mass balance for the steam side is given by:

$$\dot{m}_{s,i} - \dot{m}_{s,o} = V_s \frac{d\rho_s}{dt} \qquad (6)$$

where $\dot{m}_{s,i}$ and $\dot{m}_{s,o}$ are the mass flow rates of the steam at the inlets and the outlets of the superheaters, respectively, V_s is the volume occupied by the steam in the superheater tubes and ρ_s is the steam density.

The pressure loss of the fluid passing through the relevant exchanger is calculated as follows:

$$P_{s,i} - P_{s,o} = \frac{\ell}{\rho_s} \dot{m}_s^2 \qquad (7)$$

where ℓ is a modified friction factor and is equivalent to the product of the Darcy-Weisbach frictional factor divided by the square of the cross-sectional area of the heat exchanger pipes.

The dynamic enthalpy balance for the fluid through the exchanges is given by:

$$\rho_s V_s \frac{dh_{ave}}{dt} = \dot{m}_{s,i} h_{s,i} - \dot{m}_{s,o} h_{s,o} + \dot{Q}_s(\dot{m}_{coal}, y_{ox}) \qquad (8)$$

where h_{ave} is the average mass specific enthalpy of the steam and is estimated by the average temperature of the inlet and the outlet steam, $h_{s,i}$ and $h_{s,o}$ are the mass specific enthalpies of steam at the inlets and the outlets, respectively, $\dot{Q}_s$ is the heat transfer to the steam in the hanging tubes and is calculated, based on the CFD modelling through the reduced order model (ROM) developed in Section 4.3, as a function of the coal feed rate $\dot{m}_{coal}$ and the volume concentration of oxygen y_{ox} entering the boiler.

3.1.3 The furnace model

Since the heat transfer to the water walls and superheaters in the combustion furnace have been covered by the CFD based ROM, then empirical equations [21] for coal combustion and heat release are not necessary. Therefore the furnace model only accounts for the mass balance, the outlet temperature and the peak temperature of the metal wall. The mass balance in the furnace is described as follows:

$$\omega_{air}\dot{m}_{airlk} + \omega_{ox}\dot{m}_{ox} + \omega_{coal}\dot{m}_{coal} = \omega_{gas}\dot{m}_{gas} + \omega_{ash}\dot{m}_{ash} \tag{9}$$

where ω is the mass fraction of relevant species, $\dot{m}_{airlk}$ is the mass flow rate of the air leakage into the furnace and a value of 16kg/s is assumed. When the system operates in the air-coal mode, $\dot{m}_{ox}$ is the mass flow rate of the feed air; when the system works in the oxy-coal mode, $\dot{m}_{ox}$ is the mass flow rate of oxidant consisting of oxygen and recycled flue gas.

Further, the gas temperature $T_{gas}(\dot{m}_{coal}, y_{ox})$ at the outlet of the furnace (immediately after the FRH) and the maximum temperature on the metal wall $T_{max}(\dot{m}_{coal}, y_{ox})$ are directly calculated by the ROM which is represented in Section 4.3.

3.1.4 Convective heat exchanger model

The convective heat exchangers are PSHV, PRHV, PRH, PSH and ECON, which are shown in Fig. 1 downstream of the FRH. The convective heat exchanger model involves a set of conservation equations. In particular, the equations for the mass balance of water/steam and gas have the same form as Eq.(6); the fractional pressure drop in both steam and gas sides is expressed by a similar equation as Eq.(7). The heat balance for the steam going through the convective heat exchangers is given as follows:

$$\rho_s V_s \frac{dh_{s,ave}}{dt} = \dot{m}_{s,i} h_{s,i} - \dot{m}_{s,o} h_{s,o} + U_s (T_w - T_{s,ave}) \qquad (10)$$

where U_s is the overall admittance factor, T_w is the temperature of the wall and $T_{s,ave}$ is the average temperature of the steam.

The heat balance for the gas side of the convective heat exchangers is given by:

$$\rho_g V_g \frac{dh_{g,ave}}{dt} = \dot{m}_{g,i} h_{g,i} - \dot{m}_{g,o} h_{g,o} + U_g (T_w - T_{g,ave}) \qquad (11)$$

and the heat balance for the wall of the convective heat exchangers is given by:

$$M_w C_{p,w} \frac{dT_w}{dt} = U_s (T_{s,ave} - T_w) + U_g (T_{g,ave} - T_w) \qquad (12)$$

where M_w is the mass of the wall and $C_{p,w}$ is the specific heat capacity of the wall material.

3.1.5 Steam turbine model

Three steam turbines are employed by the power plant, including a single-stage high pressure turbine, a single-stage intermediate pressure turbine and a three-stage low pressure turbine. Each turbine stage is approximated via a single cylinder model. The relation between the expansion ratio and the steam mass flow rate is given by:

$$\dot{M}_i^2 = b_1^2 \frac{P_i^2}{T_i} (1 - r^{\frac{\gamma+1}{\gamma}}) \qquad (13)$$

and the enthalpy loss due to the polytrophic expansion in the turbine is given by:

$$h_i - h_o = b_2 T_i (1 - r^{\frac{\gamma-1}{\gamma}}) \qquad (14)$$

The electrical power output by each turbine stage is calculated as follows:

$$\dot{Q}_{gen} = b_3 \dot{M}_i (h_i - h_o) \qquad (15)$$

where the model coefficients, namely b_1, b_2 and b_3, are dimensional scaling coefficients.

3.2 The CFD furnace modelling

The CFD furnace model covers the modelling of the boiler from the burner inlets up to the exit of the reheater FRH, see Figs. 2, as used by the Didcot-A Power plant. The dimensions and details of the boiler have been given in our previous publications [21, 28]. The dimensions of the modelled boiler section are approximately 50m (height) × 30m (width) × 9m (depth) and the boiler is symmetrical, only half of the boiler is modelled. The coloured components in Fig. 2 are the superheaters, namely platen 1, platen 2, the secondary superheater (SSH) and the final reheater (FRH). The boiler employs 48 Doosan Babcock Mark-III low NO_X burners and each burner contains three annular inlets, which are the primary, secondary and tertiary inlets as shown in Fig. 2. The coal enters the boiler via the primary registers and the swirled air flows are delivered by the secondary and the tertiary registers. Further, as before, the burner geometry is slightly simplified to reduce the overall computational cost. The coal used is the world trade Pittsburgh 8 coal and its properties are summarised in Table 3.
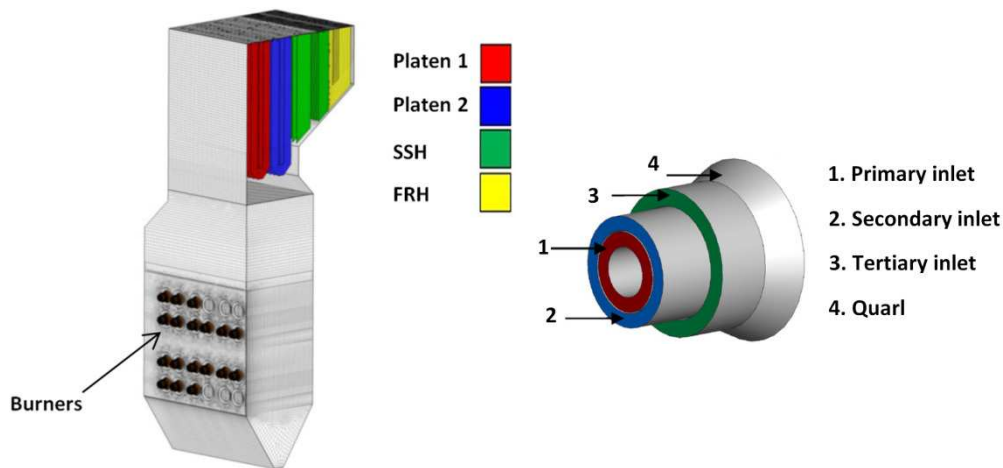
Fig. 2 Half of the geometry of the boiler (left) and its burner (right).

Table 3. Coal properties.

Coal type: Pittsburgh 8			
Ultimate analysis (wt%)		Proximate analysis (wt%)	
Carbon	83.4	Fixed carbon	50.3
Hydrogen	5.5	Volatile matter	31.0
Nitrogen	1.6	Ash	10.3
Sulphur	2.6	Moisture	8.4
Oxygen	6.9	GCV (MJ/kg)	27.3

The commercial CFD software package ANSYS FLUENT 14.0 is employed to perform the CFD simulations. The fluid flow and combustion process is modelled using the Euler-Lagrange approach [29]. The governing equations for the conservations of mass, momentum, energy and species are solved [29]. The steady state Reynolds Averaged Navier-Stokes (RANS) approach is used and the

turbulence is modelled by the realizable $k - \varepsilon$ method, which has been successfully applied previously in many coal combustion simulations [18, 30-32]. The sub-models for the coal combustion used in this CFD approach are reported in Szuhánszki et al. [30]. The correlation for the gas radiation absorption coefficient suggested by Johansson [33] was applied via user designed functions (UDF).

4. The ROM development

In order to determine the feasible operating conditions of the "retrofitted" Didcot A power unit, and in particular to determine the safe operation regime of the plant under retrofitted oxy-firing conditions, numerous plant performances have to be simulated with the whole plant model discussed in Section 3 at different operating conditions in order to cover the whole range of possible scenarios. Each of these simulated conditions requires a CFD simulation and this will be prohibitively expensive. In fact it is impossible to obtain exhaustive values of data at every desired point. Therefore the development of a reduced order model based on the advanced interpolation of a limited number of CFD simulations is desired which can be integrated into the full plant process simulations. A simple solution to this is to use linear interpolation. However, the heat transfer in the boiler is highly non-linear with respect to the coal feed rate and/or oxygen concentration. Lang et al. [34] employed a principal component analysis (PCA) with a neural network mapping technique to develop the ROMs to interpolate the flow field inside a gasifier and results with satisfying fidelity were obtained. However, this approach is quite complicated in its mathematical form. Kriging is a response surface method for spatial data interpolation and is widely used in the area of geology and aerology research [35-38]. Kriging uses spatial relationships of known points and their distribution to predict an unknown point, and it is a statistical, unbiased, and minimum variance predictor in which errors can be determined at specified points. This results in the non-linear characteristics of the data being preserved and therefore in this paper, the Kriging method is employed to build the ROMs.

4.1 Kriging interpolation

Detailed introductions to the Kriging interpolation procedure can be found in many existing publications [35-38]. In the Kriging system, the response $Y(x)$ is expressed as the following regression model:

$$Y(x) = \mathbf{f}^{T}(x)\boldsymbol{\beta} + E(x) \tag{16}$$

where $\mathbf{f}(x) = [f_1(x), f_2(x),...,f_m(x)]^T$, $\boldsymbol{\beta} = [\beta_1, \beta_2,...,\beta_m]^T$ and m is the number of the basic functions in the regression model, $Y(x)$ is the unknown function of interest, $f(x)$ is a known function of x, $\boldsymbol{\beta}$ is the regression coefficient vector, and $E(x)$ is assumed to be a stochastic process having zero mean and covariance which is written as follows:

$$Cov(x_i, x_j) = \sigma^2 R(x_i, x_j), \quad i, j = 1, 2, ..., n \tag{17}$$

where n denotes the number of the sample points, $R(x_i, x_j)$ is the correlation function and σ^2 is the process variance. The first term on the right hand side of Eq.(16), $\mathbf{f}^T(x)\boldsymbol{\beta}$, is the mean structure of the response and the second term $E(x)$ is used to model the deviation from the mean structure.

Consider n sample points, $\mathbf{x} = [x_1, x_2,...,x_n]$ with $x_i \in R^P$, P is the number of the design variables. Therefore, x is a $n \times P$ design matrix. The corresponding n responses are noted by $Y = [y(x_1), y(x_2),...,y(x_n)]$. From these sampled responses, the unknown parameters $\boldsymbol{\beta}$ and σ^2 can be estimated from the generalized least square regression:

$$\hat{\boldsymbol{\beta}} = (\mathbf{F}^T \mathbf{R}^{-1} \mathbf{F})^{-1} \mathbf{F}^T \mathbf{R}^{-1} \mathbf{Y} \tag{18}$$

$$\hat{\sigma}^2 = \frac{1}{n}(\mathbf{Y} - \mathbf{F}\hat{\boldsymbol{\beta}})^T \mathbf{R}^{-1}(\mathbf{Y} - \mathbf{F}\hat{\boldsymbol{\beta}}) \tag{19}$$

where $\mathbf{F}$ is a vector including the values of $f(x)$ evaluated at the sample points and $\mathbf{R}$ is the correlation matrix, which is composed of the correlation function evaluated at each possible combination of the sample points:

$$\mathbf{R} = \begin{bmatrix} R(x_1, x_1) & \cdots & R(x_1, x_n) \\ \vdots & \ddots & \vdots \\ R(x_n, x_1) & \cdots & R(x_n, x_n) \end{bmatrix} \tag{20}$$

The Gaussian form correlation function is widely used in engineering problems and may be expressed as follows:

$$R(x_i, x_j) = \exp\left[-\sum_{k=1}^{p} \theta_k (x_i^k - x_j^k)^2\right] \tag{21}$$

where x_i^k is the kth component of the sample point. The parameter $\boldsymbol{\theta}$ is estimated by using a maximum likelihood estimation, and the problem converts to the minimization of the following function:

$$\Gamma(\mathbf{\theta}) = \frac{1}{2}\left[\ln|\mathbf{R}| + n\ln(\hat{\sigma}^2)\right] \tag{22}$$

For an estimation of these parameters, the best linear unbiased prediction of the response at x is given by:

$$\hat{y}(x) = \mathbf{f}^T(x)\hat{\mathbf{\beta}} + \mathbf{r}^T(x)\mathbf{R}(\mathbf{Y} - \mathbf{F}\hat{\mathbf{\beta}}) \tag{23}$$

where $\mathbf{r}^T(x)$ is a vector representing the correlation between the unknown point x and all known sample points:

$$\mathbf{r}^T(x) = \left[R(x, x_1), R(x, x_2), ..., R(x, x_n)\right] \tag{24}$$

4.2 Design of experiments (DOE) for the ROM development

DOE is the preparation for the ROM development and its main task is to properly and efficiently design the sampling points so that the ROM developed can accurately represent the original physical models in the design space. Numerous sampling approaches have been developed, such as Latin Hypercube Design [39], Full Factorial Design [40], Fractional Factorial Design [41] and Orthogonal Arrays Design [42]. In this paper, the Orthogonal Arrays Design approach is used in this study because it is comparatively easy to realize when the numbers of the design variables are moderate; more importantly, the orderliness of the obtained sampling points provides the convenience for comparison and analysis.

The design variables for the ROMs are the coal feed rate and the oxygen molar concentration of the oxidant gas mixture entering the boiler, which both highly affect the fluid dynamics, combustion and heat transfer in the furnace. The information required to drive the whole plant simulation, i.e. the heat transfer rate to the water wall and superheaters, the gas temperature leaving the boiler and the peak temperature on the metal wall of the boiler, are set as the responses of the ROMs.

The coal feed rate for the full load operation (500WM$_e$) of the original air-coal plant is 46.7kg/s [28]. It is important for a power plant to be able to operate flexibly to follow as much as possible the fluctuating demand. However, a power plant cannot operate at a condition below its base load factor, which is between 60% and 70% [43] for Didcot A corresponding to a partial load of 350WM$_e$, or a coal feed rate around 33kg/s. Therefore this is the lower limit of the operating conditions investigated in this paper. Therefore, for the full consideration of the possible working range, as well as the

flexible operation of the plant, in the design space then the coal feed rate is set between 31.7kg/s and 51.7kg/s. This ensures that the full operational range of 350-500 MW_e is covered, and the design space of the oxygen molar concentration varies from 21% to 35%.

Within the identified design space, the Orthogonal Arrays Design approach is performed in terms of both the thermal inputs and the oxygen enrichments so that twenty oxy-coal and five air-coal cases are selected, as summarised in Table 4. The ASU was assumed to provide an oxygen purity of 95%, with 5% inert gases. The oxidant gas stream flow rate is determined so that an oxygen concentration at the boiler exit of 5% by volume (dry basis) is achieved. Air leakage into the boiler was assumed to be 16 kg/s and this was assumed to come through the ash hopper [30]. The flue gas is recycled on a wet basis. The coal and primary air/gas enters the furnace at a temperature of 363 K and the swirled secondary and tertiary air/gas is preheated to a temperature of 530 K.

Table 4 Operating conditions of the sampling points for the CFD simulations of the furnace

Coal, kg/s	O₂, vol%	Air-coal	21	25	30	35
51.7	Recycle ratio, %	0	76.4	71.3	65.1	59.1
	Gas mass flow, kg/s	599.9	688.4	555.9	447.2	373.3
	Excess O₂, vol%	5	5	5	5	5
	Air leakage, kg/s	16	16	16	16	16
46.7	Recycle ratio, %	0	76.2	71.0	64.8	58.8
	Gas mass flow, kg/s	540.3	619.3	500.1	402.3	335.9
	Excess O₂, vol%	5.0	5.0	5.0	5.0	5.0
	Air leakage, kg/s	16	16	16	16	16
41.7	Recycle ratio, %	0	75.9	70.7	64.5	58.4
	Gas mass flow, kg/s	480.8	550.2	444.3	357.4	298.4
	Excess O₂, vol%	5.0	5.0	5.0	5.0	5.0
	Air leakage, kg/s	16	16	16	16	16
36.7	Recycle ratio, %	0	75.5	70.3	64.0	58.0
	Gas mass flow, kg/s	421.2	481.2	388.5	312.5	260.9
	Excess O₂, vol%	5.0	5.0	5.0	5.0	5.0
	Air leakage, kg/s	16	16	16	16	16
31.7	Recycle ratio, %	0	75.1	69.8	63.4	57.3
	Gas mass flow, kg/s	361.6	412.2	332.7	267.7	223.5
	Excess O₂, vol%	5.0	5.0	5.0	5.0	5.0
	Air leakage, kg/s	16	16	16	16	16

The CFD model results for the heat transfer to the water wall and superheaters, the furnace exit temperature and the peak wall temperature of these sampling cases are listed in Table 4, which are required for the integrated full plant simulation, are summarised in Table 5.

It should be noted that the CFD model has been validated by comparing the model predictions for the air-coal 46.7 kg/s case listed in Table 4, with the in-house data from RWE npower, and they are in good agreement with a maximum discrepancy of ±5%. The validation has been reported in our previous publication [30] and thus not repeated in this paper.

The CFD predicted results shown in Table 5 for the cases investigated indicate that the total heat transfer to the water walls and the superheaters are in general close to the data of the designed air-coal cases when the oxygen concentration lies within the range 25% - 30%, and this is in-line with the previous numerical and experimental results reported in the literature [28, 30, 44]. At the oxygen concentration of 21%, the total heat transfer values are about 10-13% lower than the corresponding air-coal cases; while at the oxygen concentration of 35%, the total heat transfer values is about 9% -15% higher than the corresponding air-coal cases. Temperature distributions in the cross sections through the third column of the burners are shown in Fig. 3 for some of the air-coal and oxy-coal cases at two coal feed rates, in order to provide an indication of the variation in the temperature distributions in the furnace at different operating conditions. Overall furnace temperatures for the oxy21 cases are lower than that of the air cases. On increase in the oxygen enrichments, the volume of the flame and the furnace temperature in general sitgnificantly increase and this would enhance the heat transfer to the water walls and also have an impact on the heat transfer to the downstream heat exchangers. The gas temperatures at furnace throat are marked out and as expected, these temperatures are observed to increase as the oxygen concentration and coal feed rate increase. The four separate rows of flames can be clearly seen, where the release and combustion of volatiles takes place. The burnout of the char particles is then completed in the regime above the volatile flames in the combined stream of hot gases rising towards the superheaters.

Table 5 Heat transfer and furnace exit temperature predictions from the boiler CFD simulations.

Coal, kg/s	O_2, vol%	Air-coal	21	25	30	35
51.7	Heat transfer to water walls, MW	472.9	370.7	432.1	508.2	567.8
	Heat transfer to super heaters, MW	425.5	414.2	455.1	479.2	467.5
	Total heat transfer, MW	898.4	784.9	887.2	987.4	1035.3
	Furnace exit temperature, K	1133.5	1141.7	1133.4	1112.1	1096.6
	Maximum wall temperature, K	1662.7	1537.8	1684	1804.8	1891.3
46.7	Heat transfer to water wall, MW	456.7	358.5	413.3	482.1	519.8
	Heat transfer to super heaters, MW	388.8	373.6	409.6	427.9	417
	Total heat transfer, MW	845.5	732.1	822.9	910	936.8
	Furnace exit temperature, K	1094.1	1112	1107	1082.8	1053.6

|						
	Maximum wall temperature, K	1623.3	1499.6	1656.9	1773.3	1842.5
41.7	Heat transfer to water wall, MW	422.1	341.3	405.8	474.8	484.1
	Heat transfer to super heaters, MW	353.9	338.8	361.9	367.8	364.9
	Total heat transfer, MW	776	680.1	767.7	842.6	849
	Furnace exit temperature, K	1069.9	1082	1072.6	1055.9	1035.4
	Maximum wall temperature, K	1578.7	1463.3	1587.3	1697.9	1785
36.7	Heat transfer to water wall, MW	401	291.7	351.6	408.5	445.3
	Heat transfer to super heaters, MW	291.1	315.1	338.3	329.4	310.4
	Total heat transfer, MW	692.1	606.8	689.9	737.9	755.7
	Furnace exit temperature, K	1040.6	1038.5	1029.6	1011.2	996.9
	Maximum wall temperature, K	1531.8	1457.4	1599.7	1678.4	1723.8
31.7	Heat transfer to water wall, MW	370.9	274.4	325.8	375.2	407.3
	Heat transfer to super heaters, MW	254.2	288.6	290.5	279.6	261.5
	Total heat transfer, MW	625.1	563	616.3	654.8	678.8
	Furnace exit temperature, K	1004.9	1008.9	994.6	983.2	978.7
	Maximum wall temperature, K	1470.8	1440.4	1555.9	1620.7	1677.1
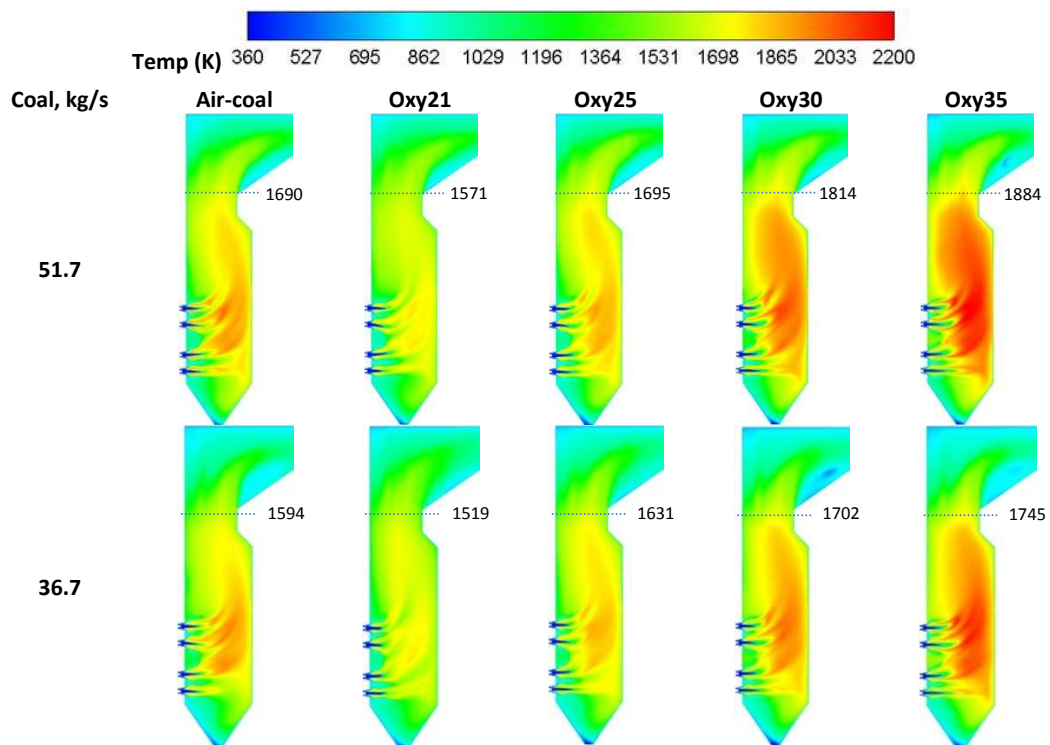
Fig. 3 Part of the predicted temperature contours inside the boiler (Oxy21 means the oxygen molar fraction of the oxidant gas entering the boiler is 21%).

4.3 The obtained ROMs

Based on the twenty oxy-coal cases performed and listed in Table 4-5, the ROMs for oxy-coal combustion of the furnace are obtained as a set of response surfaces using the Kriging regression;

with the coal feed rate varying from 31 kg/s to 52 kg/s and oxygen concentration varying from 21% to 35% (or 0.21 to 0.35). These ROMs are obtained as a set of response surfaces and respectively shown graphically in Fig. 4 and will be used to model the transfer to the water/steam side of different heat transfer components inside the furnace, namely the water wall (Fig. 4-(a)), platen 1 (Fig. 4-(b)), platen 2 (Fig. 4-(c)), SSH (Fig. 4-(d)) and FRH (Fig. 4-(e)). In addition, the ROMs for the exit gas temperature (Fig. 4-(f)) and the peak temperature on the furnace wall (Fig. 4-(g)) are also developed in order to drive the full plant simulation. Response surfaces for air-firing may also be built and in this case the surfaces reduce to curves as show in Fig. 5 and The air-coal ROMs only take the coal feed rate as design variable, also varying from 31 kg/s to 52kg/s. For simplicity, only the ROMs for heat transfer to water wall and the outlet gas temperature are presented.
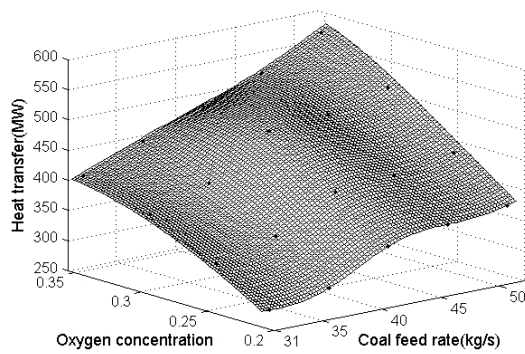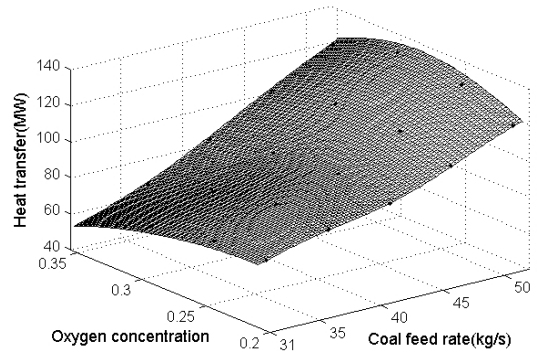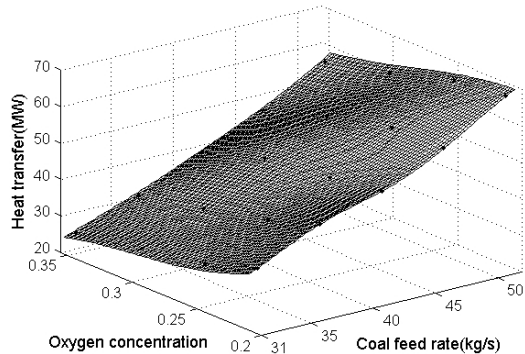

(a) Heat transfer to the water wall.
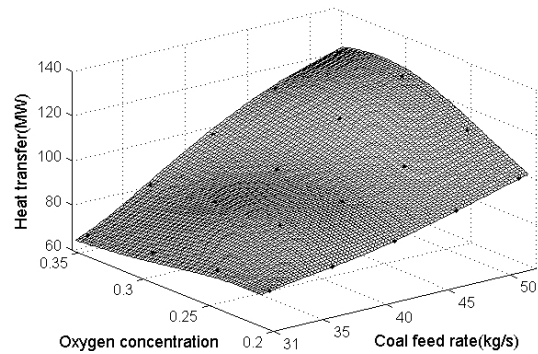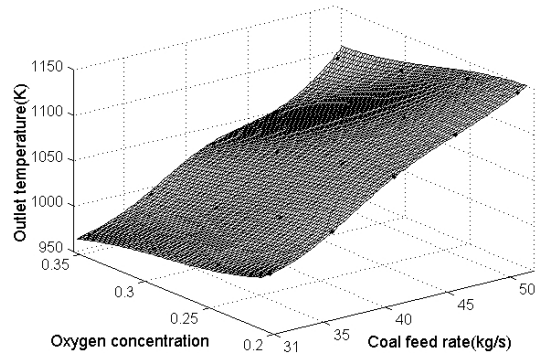
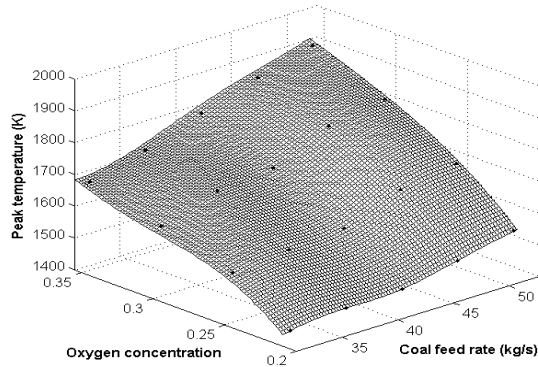(b) Heat transfer to platen 1.
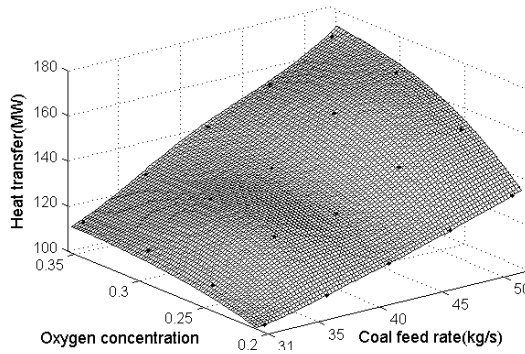
(c) Heat transfer to platen 2.

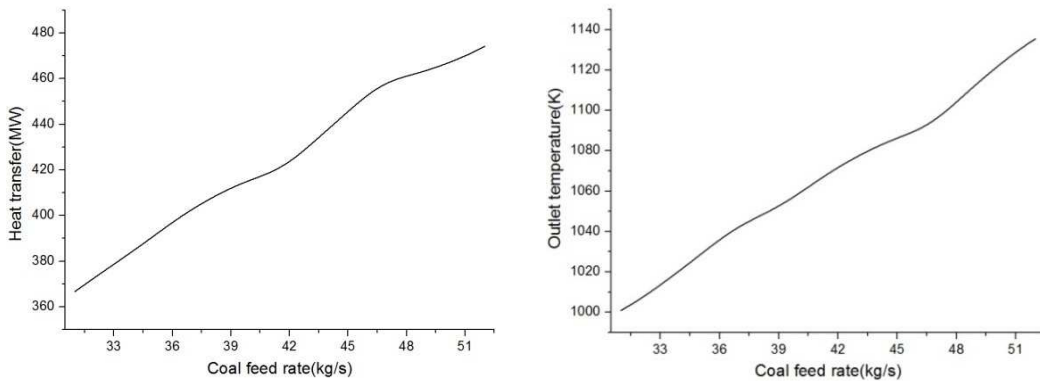(d) Heat transfer to SSH.

(e) Heat transfer to FRH.

(f) Outlet temperature.

(g) Peak temperature on the metal wall.
Fig. 4 ROMs for oxy-coal combustion of the boiler.

(a) Heat transfer to the water wall. (b) Outlet temperature.
Fig. 5 ROMs for air-coal combustion of the boiler.

As expected, the spatial nonlinearity of these ROMs respect to the oxygen concentration and coal feed rate is clear. Therefore, a nonlinear interpolation method, such as Kriging, is required to represent the nonlinearity in developing the ROMs. In general, the heat transfer and temperatures increase as the coal feed rate increases. The changes in the coal feed rate and oxygen concentration on the one hand affect the thermal properties of the combustion gas, such as specific heat and radiation absorption capability, and on the other hand impact on the flow field in the furnace, such as velocity profiles, since the gas mass flow rate needs to vary accordingly. A combination of these two aspects leads to different trends at different coal feed rate conditions: (i) at a high coal feed rate, the heat transfer to water wall, platen 1, platen 2 and SSH generally increases as the oxygen concentration increases; (ii) however, in the low coal feed rate regime, the heat transfer to platen 1 and SSH presents a decreasing trend as oxygen concentration increases, this is mainly due to the change in the flow field. As for the heat transfer to the FRH, the heat transfer reduces throughout the design space as the oxygen concentration increases; this is because in each coal feed rate condition, the total heat transfer to the upstream water wall and superheaters is predicted to increase as oxygen concentration increases, thus less heat is carried by the flue gas travelling through the FRH, which is the last heat exchange

component considered in the CFD modelling; and accordingly, the gas temperature at the outlet shows a similar decreasing trend. Further, the peak temperature of the furnace wall, including water wall and superheaters, provides important safety information as to whether the wall temperature goes beyond the limit of the tube material and the peak temperature is predicted to be located on the bottom of the superheater platen 2.

4.4 Validation of the ROMs

In order to validate the accuracy of the ROMs, four additional CFD oxy-coal cases (cases 1-4) , see Table 6, and two extra air-coal cases (cases 5, 6), see Table 6, are randomly chosen and calculated and the results obtained are compared to the ROMs values. The comparisons of the results from CFD and ROMs are summarised in Table 7. The maximum relative error between the results from CFD and ROMs is within $\pm 4\%$, and therefore the ROMs are considered to be sufficiently accurate to be used in calculating the heat transfer, outlet temperature and maximum temperature on the metal wall within the modelled range. With the newly developed ROMs, the heat transfer and temperature values can be calculated very efficiently and the CPU time is negligible in comparison to CFD simulations.

Table 6 Coal feed rates and oxygen concentrations of the validation cases.

	Case 1	Case 2	Case 3	Case 4	Case 5	Case 6
Coal feed rate (kg/s)	35.0	38.0	43.0	46.7	39.0	50.0
O_2 concentration	0.24	0.23	0.27	0.325	air	air

Table 7 Comparisons of heat transfer and temperature predictions between the CFD and ROMs.

		Water wall (MW)	Platen1 (MW)	Platen2 (MW)	SSH (MW)	FRH (MW)	Outlet T (K)	Max T (K)
Case 1	CFD	328.1	86.7	115.1	86.1	39.3	1017.1	1560.2
	ROMs	323.8	83.9	117.5	83.6	38.2	1018.5	1549.2
	error	-1.3%	-3.2%	2.1%	-3.0%	-2.2%	0.1%	-1.0%
Case 2	CFD	330.8	89.5	120.6	90.6	45.2	1045.6	1534.1
	ROMs	336.3	86.3	118.6	88.6	43.7	1046.3	1520.0
	error	1.7%	-3.6%	-1.7%	-2.2%	-3.3%	0.1%	-1.0%
Case 3	CFD	431.4	99.2	136.7	95.5	48.8	1074.8	1675.5
	ROMs	444.2	95.9	134.1	98.5	49.0	1076.7	1652.3
	error	3.0%	-3.3%	-1.9%	3.1%	0.4%	0.2%	-1.4%
Case 4	CFD	509.1	112.4	156.2	111.2	49.7	1069.3	1812.9
	ROMs	506.7	112.9	154.6	108.4	49.5	1067.4	1810.1
	error	-0.5%	0.4%	-1.0%	-2.5%	-0.4%	-0.2%	-0.2%
Case 5	CFD	406.2	82.2	115.4	81.0	40.2	1050.9	1566.8
	ROMs	412.0	81.9	115.0	79.4	40.2	1052.7	1553.8

	error	1.4%	-0.4%	-0.3%	-2.0%	0.0	0.2%	-1.0%
Case 6	CFD	469.2	98.8	137	110.5	59.3	1125.5	1641.7
	ROMs	466.5	102	139.1	113.3	58.7	1121.1	1650.2
	error	-0.6%	3.2%	1.5%	2.5%	-1.0%	-0.4%	1.0%

5. Model validation and discussions on the whole plant co-simulations

5.1 Validation of the integrated CFD/process full plant model

This integrated full plant model is validated by comparing the results obtained to those obtained from RWE's in-house code MOPEDS, which was developed for modelling the air-coal firing of the power plant and only full load air-coal firing simulation results are available. The predicted steam/water and gas temperatures entering and leaving the heat exchangers are shown in Table 8, where the values in the brackets are the results obtained by MOPEDS and the other results are from this integrated CFD/process model. Since the gas side temperatures of the superheaters are considered in the CFD model rather than the full plant model, the gas temperature for platen 1, platen 2, SSH and FRH are not compared. Table 8 indicates that the maximum relative difference between the results from MOPEDS and the integrated CFD/process model is found be the temperature of the gas at the inlet of the economiser (Econ), which is about 4%. The predicted results of the steam generation mass flow rate, steam pressure and steam temperature in the steam drum are compared in Table 9, showing the relative errors are within $\pm 1\%$. Considering that MOPEDS was built on measurements for this particular type of furnace, it is considered to be reliable and therefore it may be concluded that this newly developed integrated full plant model can give reasonable representations of the real power plant.

Table 8. A comparison in the predictions of MOPEDS and the full plant model for the heat exchangers.

	Temperatures (K) (values in brackets are the MOPEDS results)			
	Water/Steam		Gas	
	T_{in}	T_{out}	T_{in}	T_{out}
Platen 1	656(654)	707(718)	-	-
Platen 2	676(682)	761(752)	-	-
SSH	761(752)	841(841)	-	-
FRH	760(736)	831(841)	-	-
PSHV	649(648)	656(654)	1091(1054)	1062(1027)
PSH	629(628)	649(648)	1062(1027)	786(756)
Econ	522(523)	579(573)	786(756)	636(621)
PRHV	706(694)	760(736)	1062(1027)	962(923)
PRH	625(638)	705(694)	961(923)	801(769)

**Table 9. A comparison in the predictions of MOPEDS and
the full plant model for the steam drum.**

	Steam generated (kg/s)	Drum pressure (bar)	Steam temperature (K)
This model	393	178	629
MOPEDS	390	178	628

5.2 Results and discussions

When a conventional coal-fired power plant is retrofitted into an oxy-coal power plant, the fundamental combustion environment in the furnace is changed, and thus impacts on the heat transfer characteristics of the boiler. In order to investigate the impact of an oxy-coal upgrade on the heat transfer and steam generation of this conventional power plant, this section analyses the simulation results of the "retrofitted" power plant under the working scenarios of air-coal, oxy21, oxy23, oxy25, oxy27.5, oxy30, oxy32.5 and oxy35 in four different electricity load levels, namely 500MW$_e$ (full load), 450MW$_e$, 400MW$_e$ and 350MW$_e$, which cover the designed full operational regime of the power plant. In these investigated power load levels, the coal consumption rates are predicted to be different and these obtained values are about 47 kg/s for 500MW$_e$ operation, 42 kg/s for 450MW$_e$ operation, 38 kg/s for 400Me operation and 33 kg/s for 350MW$_e$ operation.

5.2.1 Impacts of oxy-coal retrofit on the evaporative heat transfer and steam generation

A key parameter describing the output capacity of a coal-fired power plant is the generated steam mass flow rate, which is dictated by the heat transfered to the water walls, namely the evaporative heat. With an oxy-coal retrofit, the original evaporative heat transfer under air-coal firing condition is changed.

The predicted evaporative heat transfer and steam generation rates from the steam drum at the four different electricity output levels are plotted in Fig. 6 as a function of oxygen concentration. For comparison, the corresponding evaporative heat values under air-coal firing mode are marked by the symbol ✕. The intersections of the vertical dashed lines and the horizontal axis are the matching points where the evaporative heat or steam generation from the steam drum under oxy-coal can be matched with the air-coal conditions. In general, the evaporative heat as the oxygen concentration rises is because the flame temperature in the combustion furnace increases when the oxygen concentration of the gas entering the boiler increases, thus the radiation to the surrounding water walls becomes more intensive. The steam generation from the steam drum is the physical phenomenon of the evaporative heat transfer and therefore t`he steam generation from the drum also increases as the

oxygen concentration increases. The steam generation can be approximately matched to air-coal firing within the oxygen concentration range of 27%-28% for the full operational range of the plant.
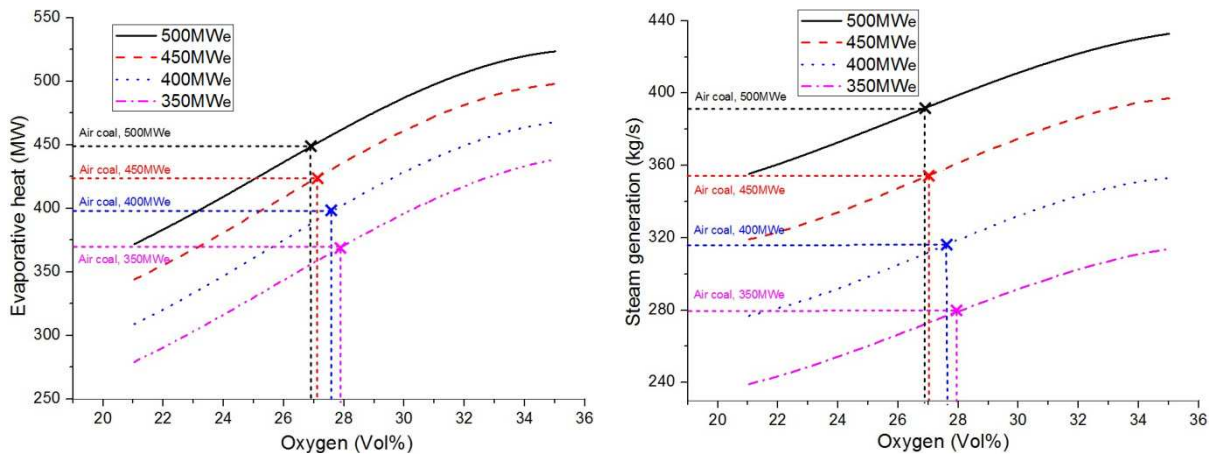
Fig. 6 The predicted evaporative heat (left) and the steam generation (right).

It should be noted that the steam generated from the steam drum is not the total steam that drives the steam turbines. Although most steam comes from the steam drum, a small amount of additional steam is brought by the external water sprayed into the superheat steam at the inlet of superheater platen 2, in order to maintain an endurable wall temperature for the superheaters. If more water spray is required then less steam would be needed from the steam drum. The total steam generated that enters the steam turbine is presented in Fig. 7, and it indicates that the total steam generation can be matched with the air-firing cases within the oxygen concentration range between 25% and 27%. It is interesting to note that when comparing the total steam generation with the steam generation from the drum shown in Fig. 6, less steam would be required from the drum when the plant is retrofitted to oxy-firing, in particular at low load conditions.
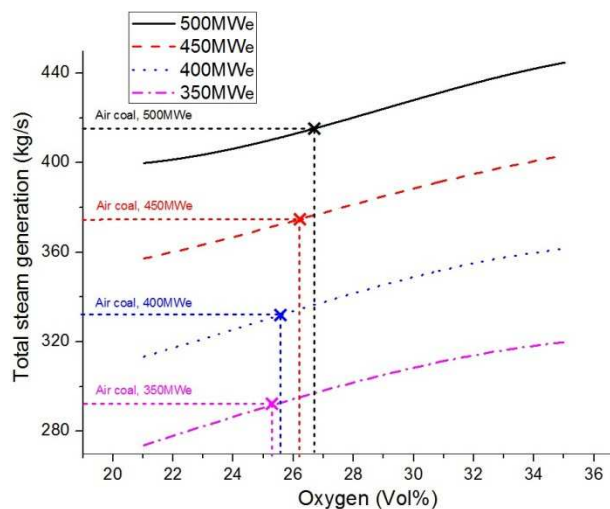
Fig. 7 The total steam generation as a function of oxygen concentration.

5.2.2 Impacts of an oxy-coal retrofit on the heat transfer inside and outside the furnace

In the furnace, where combustion of coal takes place, the heat transfer to the water wall, platen superheaters and the reheater (platen 1, platen 2, SSH and FRH shown in Fig. 1), which are calculated from the CFD ROMs, are dominated by radition, i.e. radiative heat transfer. As the flue gas comes out from the furnace, the gas temperature is about 1100 K (for 500MW$_e$ operation) or even lower, and the steam/water temperatures in the downstream heat exchangers (PSHV, PRHV, PRH, PSH and ECON shown in Fig. 1) vary from 600 to 800 K. Thus radiation is not considered the dominant form of heat transfer [21] but by convective heat transfer. Fig. 8 compares both the contributions of the radiative and convective heat transfers to the steam generation cycle. Clearly, the radiative heat dominates the process and it increases as the oxygen concentration increases while the opposite trend can be observed for the convective part. As the oxygen concentration increases, the gas temperature increases so that the radiation is also strengthened [28, 30]. On the other hand, (i) as the oxygen concentration increases, the recycle ratio of the flue gas decreases, leading to a lower mass flow rate of the flue gas going through the convective heat exchangers; (ii) as the oxygen concentration increases, the gas temperature leaving the final reheater (FRH), which is the last heat transfer component considered in the CFD model, decreases since the total heat input to the furnace is kept almost constant. These two factors cause a decrease in the internal heat carried by the flue gas that goes through the convective heat exchangers.
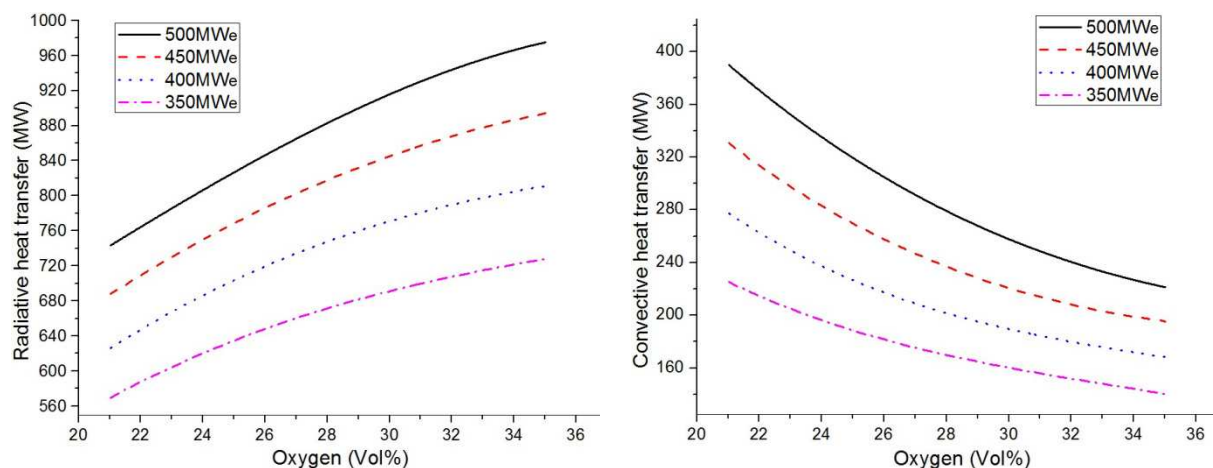

Fig. 8 The radiative heat transfer (left) and convective heat transfer to the water/steam cycle (right).

5.2.3 Impacts of oxy-coal retrofit on the steam temperatures

In the super heat region of the boiler, the super heat steam passes through the platen 1, water sprayer, platen 2 and SSH sequentially. In addition to investigate the heat transfer from the gas side, it is of

interest to look into the steam temperature change along these super heat components on the steam side, therefore the predicted steam temperatures at the inlet/outlet of these elements are presented in Fig. 9 in a sequential order that steam goes through, and they are linked with straight lines in order to show the general trend of the temperature variations. In addition, only the 500MW$_e$ and 400MW$_e$ simulation results are presented, since the 450MW$_e$ and 350MW$_e$ results show similar patterns. In general, the steam temperatures increase as the super heat steam passes through platen 1 to SSH. A significant drops are observed in the water sprayer where the super heat steam mixes with the sprayed water so that the downstream steam temperature would not become too high to protect the metal tubes, and this is achieved by a PI controller, to maintain the steam temperature at the outlet of the SSH to the control target of approximately 841 K. The steam temperatures in platen 2 and SSH are predicted to be very close for all cases investigated; while the biggest temperature differences are observed in platen 1 and water sprayer.


(a) Predictions for 500M$_e$ operation (b) Predictions for 400M$_e$ operation
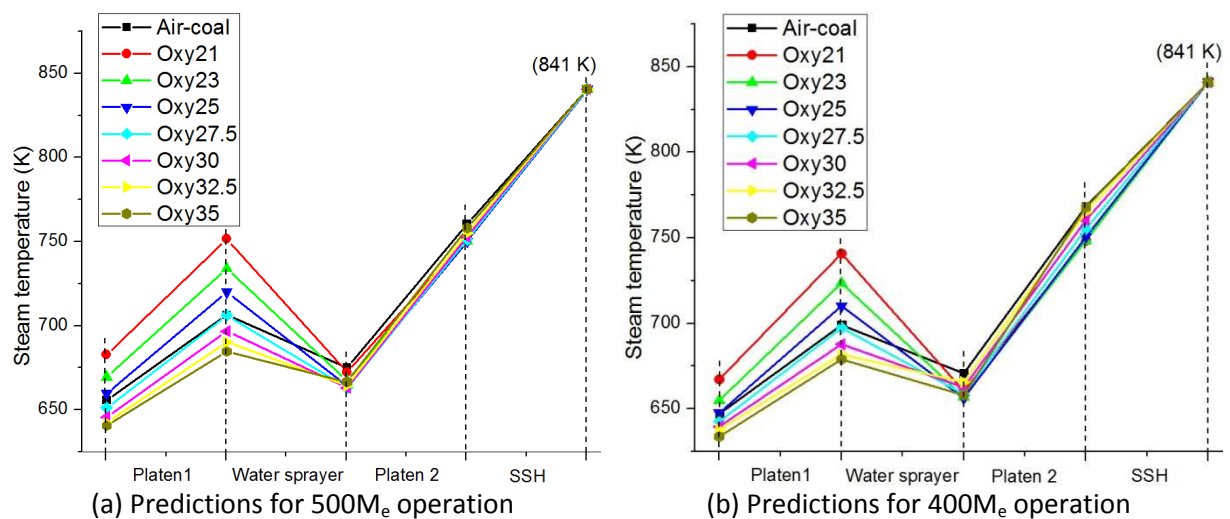
Fig. 9 Predicted steam temperatures at the inlet/outlet of the super heat components.

5.2.4 Impacts of oxy-coal retrofit on the peak wall temperature: a safety issue

As discussed in Section 4.3, the peak wall temperature was predicted to be located at the bottom of the superheater platen 2. Under air-firing, the highest wall temperature is approximately 1620 K at full load, see Fig. 10. It is important to note that the predicted peak temperatures of the tube wall under oxy-coal firing are higher than 1620 K under full load air-coal firing when the oxygen concentrations are higher than about 23.5% for 500MW$_e$, 25% for 450MW$_e$, 27% for 400MW$_e$ and 29% for 350MW$_e$, as is shown in Fig. 10. If the retrofitted unit is to be operated at an oxygen level of 25%-27% then: (i) for the full load operation of 500MW$_e$, the temperature increase is approximately 60 (for 25%)-100 (for 27%) K above 1620 K; (ii) for the partial load condition of 450MW$_e$, the temperature increase is

negligible at the oxygen level of 25%, but gradually increases to 70 K at the oxygen level of 27%; (iii) for other partial load conditions of 400MW$_e$ and 350MW$_e$, the peak temperature increases will be lower than 1620 K for oxygen concentrations of 25%-27%.

Therefore, attention must be paid when this retrofitted power plant operates beyond 450MW$_e$, due to the temperature increase. If the tube material of platen 2 cannot endure the temperature increase, then an upgrade on the material is required.
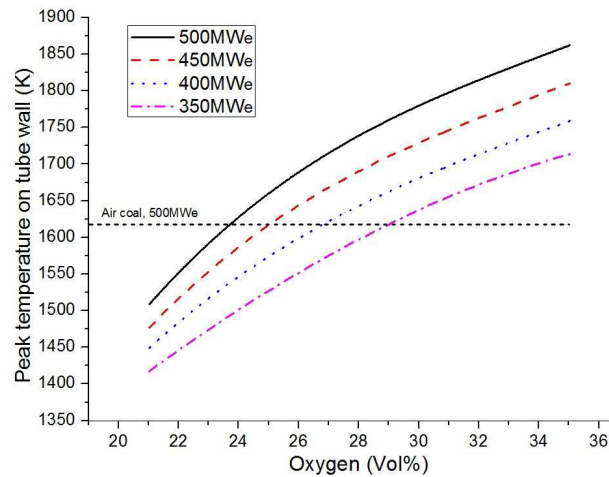
Fig. 10 Predicted peak temperatures on the tube wall.

6. Summary and conclusions

This paper investigates the potential of retrofitting a conventional air-coal power plant to oxy-coal firing and the possible required inlet oxygen concentrations to achieve a similar plant performance to that of air-coal firing. An integrated full plant co-simulation model has been developed. In order to accurately model the heat transfer and temperature characteristics in the furnace, a high fidelity CFD method is used to account for the fluid dynamics, combustion, and heat transfer inside the furnace. Then a set of fast reduced order models (ROMs) has been built using the Kriging method which can be efficiently integrated into the process model.

A range of air-coal and oxy-coal conditions in different power loads from 350MW$_e$ to 500MW$_e$ has been simulated. The results indicate that it is possible to retrofit the air-coal firing power plant to oxy-coal firing and achieve the original designed performances of the power plant in air-coal firing. However, the impact of the retrofit is expected to be different for different parts of the plant. The biggest impacts observed are to the steam generation from the steam drum and the steam temperature at the exit of the super heater platen 1. It is suggested that an oxygen enrichment range of 25%-27%

would be adequate for the retrofitted plant to match the performance achievable under air-firing for the full operational load regime of the plant. Clearly, optimisation of the retrofitted plant would be required to determine the optimal oxygen enrichment for each particular load. The peak temperature would increase in the oxy-coal mode, in particular on the superheater platen 2. If the tube material cannot endure the temperature increase, then an upgrade on the material may be required.

Acknowledgements

Reference

[1] L. Zheng, Oxy-Fuel Combustion for Power Generation and Carbon Dioxide (CO_2) Capture, Woodhead Publishing Limited, UK, 2011.

[2] J. Xiong, H. Zhao, C. Zheng, Exergy Analysis of a 600 MWe Oxy-combustion Pulverized-Coal-Fired Power Plant, Energ Fuel, 25 (2011) 3854-3864.

[3] X. Pei, B. He, L. Yan, C. Wang, W. Song, J. Song, Process simulation of oxy-fuel combustion for a 300MW pulverized coal-fired power plant using Aspen Plus, Energ Convers Manage, 76 (2013) 581-587.

[4] T.G. Chao Fu, Heat Integration of an Oxy-Combustion Process for Coal-Fired Power Plants with CO2 Capture by Pinch Analysis, Chemical Engineering Transactions, 21 (2010) 181-186.

[5] A.H. Al-Abbas, J. Naser, D. Dodds, CFD modelling of air-fired and oxy-fuel combustion of lignite in a 100KW furnace, Fuel, 90 (2011) 1778-1795.

[6] G.M. Álvarez L., Pourkashanian M., Williams A., Riaza J., Pevida C., Pis J. J., Rubiera F., CFD modelling of oxy-coal combustion in an entrained flow reactor, Fuel Processing Technology, 92 (2011) 1489-1497.

[7] E.L.K. Buhre B. J. P., Sheng C. D., Gupta R. P., Wall T. F., Oxy-fuel combustion technology for coal-fired power generation, Progress in Energy and Combustion Science, 31 (2005) 283-307.

[8] L. Chen, S.Z. Yong, A.F. Ghoniem, Oxy-fuel combustion of pulverized coal: Characterization, fundamentals, stabilization and CFD modeling, Progress in Energy and Combustion Science, 38 (2012) 156-214.

[9] I.R.M.A. Gharebaghi M., Ma L., Pourkashanian M., Pranzitelli A., Large eddy simulation of oxy-coal combustion in an industrial combustion test facility, International Journal of Greenhouse Gas Control, 5, Supplement 1 (2011) S100-S110.

[10] Z.C. Zhou Wu, Duan Lunbo, Liu Daoyin, Chen Xiaoping, CFD modeling of oxy-coal combustion in circulating fluidized bed, International Journal of Greenhouse Gas Control, 5 (2011) 1489-1497.

[11] L. Álvarez, M. Gharebaghi, M. Pourkashanian, A. Williams, J. Riaza, C. Pevida, J.J. Pis, F. Rubiera, CFD modelling of oxy-coal combustion in an entrained flow reactor, Fuel Processing Technology, 92 (2011) 1489-1497.

[12] I. Constenla, J.L. Ferrín, L. Saavedra, Numerical study of a 350MWe tangentially fired pulverized coal furnace of the As Pontes Power Plant, Fuel Processing Technology, 116 (2013) 189-200.

[13] P. Warzecha, A. Boguslawski, Simulations of pulverized coal oxy-combustion in swirl burner using RANS and LES methods, Fuel Processing Technology, 119 (2014) 130-135.

[14] S.R. Gubba, D.B. Ingham, K.J. Larsen, L. Ma, M. Pourkashanian, H.Z. Tan, A. Williams, H. Zhou, Numerical modelling of the co-firing of pulverised coal and straw in a 300 MWe tangentially fired boiler, Fuel Processing Technology, 104 (2012) 181-188.

[15] S.E. Zitney, Process/equipment co-simulation for design and analysis of advanced energy systems, Comput Chem Eng, 34 (2010) 1532-1542.

[16] F.W. Sloan D, Zitney S, Syamlal M, Power plant simulations using process analysis software linked to advanced modules, in: In: Proceedings of the 29th international technical conference on coal utilization & fuel systems, Clearwater, FL, 2004.

[17] L.I. Díez, C. Cortés, A. Campo, Modelling of pulverized coal boilers: review and validation of on-line simulation techniques, Applied Thermal Engineering, 25 (2005) 1516-1533.

[18] H.P.J. Edge P. J., Pourkashanian M., Stephenson P. L., Integrated fluid dynamics-process modelling of a coal-fired power plant with carbon capture, Applied Thermal Engineering, 60 (2013) 456-464.

[19]   http://www.rwe.com/web/cms/en/320870/rwe-npower/about-us/our-businesses/power-generation/didcot/didcot-a/, in.

[20] M.L. Stein, Interpolation of Spatial Data: Some Theory for Kriging, Springer, Chicago, USA, 1999.

[21] H.P.J. Edge P. J., Pourkashanian, M., Stephenson P. L., Williams A., A reduced order full plant model for oxyfuel combustion, Fuel, 101 (2012) 234-243.

[22] D.J. Hersh, J.M. Abrardo, Air Separation Plant Design, Cryogenics, 17 (1977) 383-390.

[23] G. Scheffknecht, L. Al-Makhadmeh, U. Schnell, J. Maier, Oxy-fuel coal combustion—A review of the current state-of-the-art, International Journal of Greenhouse Gas Control, 5, Supplement 1 (2011) S16-S35.

[24] K.S. Bhambare, S.K. Mitra, U.N. Gaitonde, Modeling of a Coal-Fired Natural Circulation Boiler, Journal of Energy Resources Technology, 129 (2006) 159-167.

[25] Z. Hasan, Dynamic modelling and simulation for coal-fired boilers, MSc thesis, in, University of Cranfield, 2008.

[26] E.J. Adam, J.L. Marchetti, Dynamic simulation of large boilers with natural recirculation, Comput Chem Eng, 23 (1999) 1031-1040.

[27] K.J. Åström, R.D. Bell, Drum-boiler dynamics, Automatica, 36 (2000) 363-378.

[28] S.J. Black S., Pranzitelli A., Ma L., Stanger P. J., Ingham D. B., Pourkashanian M., Effects of firing coal and biomass under oxy-fuel conditions in a power plant boiler using CFD modelling, Fuel, 113 (2013) 780-786.

[29] I. ANSYS, ANSYS FLUENT Theory Guide, Release 14.0, in, 2011.

[30] B. Szuhánszki J., S., Pranzitelli A., Ma L., Stanger P. J., Ingham D. B., Pourkashanian M., Evaluation of the Performance of a Power Plant Boiler Firing Coal, Biomass and a Blend Under Oxy-fuel Conditions as a CO2 Capture Technique, Energy Procedia, 37 (2013) 1413-1422.

[31] H.P.J. Edge P. J., Pourkashanian M., Williams A., An integrated computational fluid dynamics–process model of natural circulation steam generation in a coal-fired power plant, Comput Chem Eng, 35 (2011) 2618-2631.

[32] T.F.W. S.P.Khare, R.P.Gupta, L.K.Elliott, B.J.P.Buhre, Retrofitting of a conventional coal fired plant to oxy-firing: heat transfer impacts for the furnace and associated oxygen level, in: 5th Asia-Pacific Conference on Combustion, 2005.

[33] L.B. Johansson Robert, Andersson Klas, Johnsson Filip, Account for variations in the H2O to CO2 molar ratio when modelling gaseous radiative heat transfer with the weighted-sum-of-grey-gases model, Combustion and Flame, 158 (2011) 893-901.

[34] M.A. Lang Y. D., Biegler L. T., Munteanu S., Madsen J. I., Zitney S. E., Reduced Order Model Based on Principal Component Analysis for Process Simulation and Optimization, Energ Fuel, 23 (2009) 1695-1706.

[35] C. Thiart, A. Stein, Continental-scale kriging of gold-bearing commodities, Spatial Statistics, 6 (2013) 57-77.

[36] G. Jia, A.A. Taflanidis, Kriging metamodeling for approximation of high-dimensional wave and surge responses in real-time storm/hurricane risk assessment, Computer Methods in Applied Mechanics and Engineering, 261–262 (2013) 24-38.

[37] R.M. Sampson Paul D., Szpiro Adam A., Bergen Silas, Sheppard Lianne, Larson Timothy V., Kaufman Joel D., A regionalized national universal kriging model using Partial Least Squares regression for estimating annual PM2.5 concentrations in epidemiology, Atmos Environ, 75 (2013) 383-392.

[38] Z. Masoomi, M.S. Mesgari, M.B. Menhaj, Modeling uncertainties in sodium spatial dispersion using a computational intelligence-based kriging method, Computers & Geosciences, 37 (2011) 1545-1554.

[39] M.D. McKay, R.J. Beckman, W.J. Conover, A Comparison of Three Methods for Selecting Values of Input Variables in the Analysis of Output From a Computer Code, Technometrics, 42 (2000) 55-61.

[40] J. Antony, 6 - Full Factorial Designs, in: J. Antony (Ed.) Design of Experiments for Engineers and Scientists (Second Edition), Elsevier, Oxford, 2014, pp. 63-85.

[41] J. Antony, 7 - Fractional Factorial Designs, in: J. Antony (Ed.) Design of Experiments for Engineers and Scientists (Second Edition), Elsevier, Oxford, 2014, pp. 87-112.

[42] E.S.L. R.N. Kacker, J.J. Filliben, Taguchi's orthogonal arrays are classical designs of experiments, Research of NIST, 96 (1991) 577-591.

[43] Operating flexibly - Didcot A makes over 750 starts in one year, in, RWE Power International.

[44] A.H. Al-Abbas, J. Naser, D. Dodds, CFD modelling of air-fired and oxy-fuel combustion in a large-scale furnace at Loy Yang A brown coal power station, Fuel, 102 (2012) 646-665.